ATLAS PUB Note
ATL-PHYS-PUB-2018-036
27th November 2018

# ATLAS sensitivity to dark matter produced in association with heavy quarks at the HL-LHC

The ATLAS Collaboration

This note presents the prospects of a search for weakly interacting dark matter produced in association with heavy flavour quarks at the HL–LHC. The search is performed assuming 3000 fb$^{-1}$ of proton-proton collisions collected by the ATLAS detector at a centre of mass energy of 14 TeV. Two experimental signatures are investigated, characterised by missing transverse momentum and either a pair of bottom quarks or two opposite-charge leptons (electrons or muons) resulting from the decay of a top quark pair or a top quark and a $W$-boson. The results are interpreted within the framework of Simplified Models which couple the dark and Standard Model sectors via the exchange of colour-neutral spin-0 mediators, assuming unitary couplings and a dark matter mass of 1 GeV. Compared to a previous search conducted with 36.1 fb$^{-1}$ of data at $\sqrt{s}$ = 13 TeV, the reach achievable for dark matter detection in events with bottom quarks is extended by a factor of 3–8.7 following the increased luminosity and centre of mass energy expected for the HL–LHC final dataset, along with the upgrades to the ATLAS detector. For events with top quarks in the final state, the expected sensitivity to scalar mediator production extents by a factor of 5, and exclusion of pseudoscalar mediator masses up to 385 GeV becomes possible.

ATL-PHYS-PUB-2018-036
28 November 2018

# 1 Introduction

While the existence of dark matter (DM) is supported by a plethora of astrophysical observations [1–4], its particle nature remains largely unexplained. The Weakly Interacting Massive Particle (WIMP) [5] is a well-motivated candidate for the bulk of dark matter, possessing the requisite properties and appearing in many Beyond the Standard Model (SM) theories. WIMPs created at colliders escape detection, resulting in a signature characterised by missing transverse momentum. Searches for WIMP dark matter, observable by the presence of an accompanying SM particle(s), have been performed extensively at the Large Hadron Collider (LHC) [6–12]. This note presents the prospects of a search for dark matter produced in association with heavy flavour (bottom or top) quarks at the High Luminosity LHC (HL–LHC).

Signatures involving heavy flavour quarks are expected to be the most sensitive to models where the dark and SM sectors couple via the exchange of a spin-0 mediator [13]. This study therefore focuses on two simplified models, defined by either a scalar, $\phi$, or pseudoscalar, $a$, mediator [14–16]. In both cases, the mediating particle is taken to be colour-neutral and the dark matter candidate is assumed to be a weakly interacting Dirac fermion, $\chi$, uncharged under the SM. The models are described by five common parameters: the dark matter mass, $m(\chi)$, the mediator mass, $m(\phi)$ or $m(a)$, the dark matter–mediator coupling, $g_\chi$, the flavour-universal SM–mediator coupling, $g_\nu$, and the decay width of the mediator, $\Gamma(\phi)$ or $\Gamma(a)$. For simplicity, an assumption of $g_\chi = g_\nu = g$ is made and the mediator width is taken to be the minimal width described in Ref. [15]. For this scenario, $\chi\bar{\chi}$ production in association with top-quarks is expected to dominate at the HL–LHC. Two signatures featuring top quarks in the final state are therefore considered. The first signature, denoted DM+$t\bar{t}$, is characterised by two tops decaying di-leptonically as shown in Figure 1(a). The second signature, DM+$Wt$, involves a single top produced in tandem with a $W$-boson, both of which decay leptonically as shown in Figures 1(b) and 1(c).

While the couplings of the mediator to the up- and down-type quarks are assumed to be indistinguishable in this study, the condition is by no means a necessary one. In the event that coupling to up-type quarks is suppressed - a possibility in UV completions of the aforementioned models - production of dark matter in association with bottom quarks becomes relevant. The DM+$b\bar{b}$ final state is also well motivated as an avenue for probing the parameter space of two-Higgs doublet models (2HDM). In the context of the 2HDM+$a$ model [17, 18] for example, the rate for $pp \rightarrow b\bar{b} + a$ is enhanced by the ratio of the Higgs doublet vacuum expectation values, $\tan\beta$, if a Yukawa sector of type-II is realised. Constraints on $\tan\beta$ can be extracted via a straightforward recasting of exclusion limits on the simplified pseudoscalar mediator model (see Appendix A in Ref. [18]). Consequently, a search for DM+$b\bar{b}$ targeting the latter model is optimised to also set bounds on $\tan\beta$. DM+$t\bar{t}$/$Wt$, mono-$X$, and di-top searches can be exploited in a similar manner, however the DM+$b\bar{b}$ channel is uniquely situated to probe the high $\tan\beta$ region, a region not currently well constrained in two-Higgs doublet models. Dark matter production in association with $b$-quarks is therefore also considered in this note, an example diagram for which is shown in Figure 1(d) where the model parameters are as defined in the previous paragraph.

A search targeting the DM+$b\bar{b}$ and DM+$t\bar{t}$ signatures was performed at the LHC using 36.1 fb$^{-1}$ of data collected in 2015 and 2016 at a centre of mass energy of 13 TeV [13]. No evidence of physics beyond the SM was found and constraints were placed on the ratio of the measurable cross-section to the theoretically predicted cross-section, $\sigma/\sigma(g = 1.0)$, as a function of the mediator mass in the range 10-500 GeV. Likewise, constraints on spin-0 mediator production with a DM+$Wt$ signature were projected for 35 fb$^{-1}$ and 300 fb$^{-1}$ of data in Ref. [19]. This note presents the prospects for further constraining these models with HL-LHC data and is divided into two independent analyses. The first is optimised for the DM+$b\bar{b}$ final state and serves to additionally quantify the expected gain in performance potential for HL–LHC

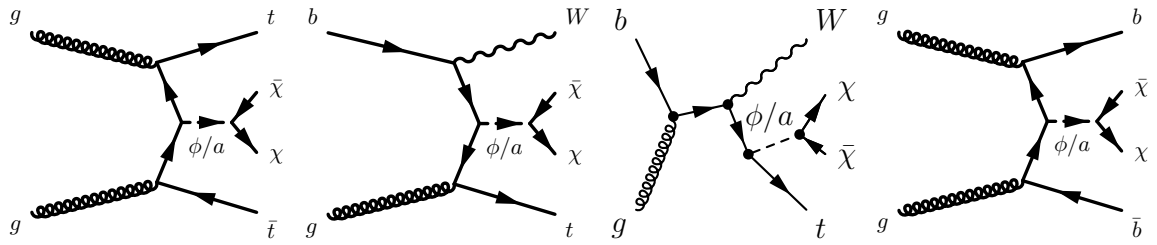


(a) DM+$t\bar{t}$ (b) DM+$Wt$ (c) DM+$Wt$ (d) DM+$b\bar{b}$

Figure 1: Representative tree-level diagrams for the production of dark matter ($\chi$) in association with (a-c) top quarks and (d) bottom quarks following the exchange of either a colour-neutral scalar ($\phi$) or pseudoscalar ($a$) particle.

searches involving flavour tagged jets and large missing transverse momentum. Similarly, the second analysis, which is optimised for the DM+$t\bar{t}$ and DM+$Wt$ final states, also serves to showcase the gain for searches featuring a combination of flavour tagged objects, missing transverse momentum, and leptons.

## 2 The LHC and HL–LHC

In the present data-taking period, the LHC delivered ~150 fb$^{-1}$ of proton-proton collisions with a peak instantaneous luminosity of $2\times10^{34}$ cm$^{-2}$s$^{-1}$ and an average number of collisions per bunch crossing of $\langle\mu\rangle \sim 35$. A long shutdown (LS2) will follow, during which the injection chain is foreseen to be modified to allow for instantaneous luminosities up to ~$2.5\times10^{34}$ cm$^{-2}$s$^{-1}$. The data collected up to the next long shutdown (LS3) will amount to ~300 fb$^{-1}$. An increase of the centre-of-mass-energy to 14 TeV is possible and is assumed to happen for this study. An upgrade of the accelerator to the HL–LHC is planned to take place during LS3, enabling luminosities of ~$7\times10^{34}$ cm$^{-2}$s$^{-1}$ to be achieved. The HL–LHC is expected to deliver an average number of pile up interactions per bunch crossing of $\langle\mu\rangle \sim 200$ during its operation with the total data collected amounting to ~3000 fb$^{-1}$.

## 3 The ATLAS Detector

The ATLAS experiment [20] is a multi-purpose particle detector with a forward-backward symmetric cylindrical geometry and nearly $4\pi$ coverage in solid angle[1]. The interaction point is surrounded by an inner detector (ID), a calorimeter system, and a muon spectrometer.

Upgrades to the detector and the triggering system are planned to adapt the experiment to the increasing instantaneous and integrated luminosities expected with the HL–LHC [21–27].

[1] ATLAS uses a right-handed coordinate system with its origin at the nominal interaction point (IP) in the centre of the detector and the $z$-axis along the beam pipe. The $x$-axis points from the IP to the centre of the LHC ring, and the $y$-axis points upward. Cylindrical coordinates ($r$, $\phi$) are used in the transverse plane, $\phi$ being the azimuthal angle around the beam pipe. The pseudorapidity is defined in terms of the polar angle $\theta$ as $\eta = -\ln\tan(\theta/2)$. Rapidity is defined as $y = 0.5\ln[(E+p_z)/(E-p_z)]$ where $E$ denotes the energy and $p_z$ is the component of the momentum along the beam direction.

In the reference upgrade scenario, the ID will provide precision tracking of charged particles for pseudorapidities $|\eta| < 4.0$ and will be surrounded by a superconducting solenoid providing a 2 T axial magnetic field. It will consist of silicon pixel and microstrip detectors.

In the pseudorapidity region $|\eta| < 3.2$, the currently installed high-granularity lead/liquid-argon (LAr) electromagnetic (EM) sampling calorimeters will be used. The current steel/scintillator tile calorimeter will be used, although the readout electronics will be replaced to enable improved triggering [23, 24]. A new high-granularity timing detector (HGTD) will also be installed in the forward regions to reduce occupancy from $|\eta| < 2.4$ up to $|\eta| < 4.0$ in the high pile-up HL-LHC environment [27].

The muon spectrometer, consisting of three large superconducting toroids with eight coils each, and a system of trigger and precision-tracking chambers, which provide triggering and tracking capabilities in the ranges $|\eta| < 2.4$ and $|\eta| < 2.7$ respectively, could be upgraded with the addition of a very forward muon tagger that would extend the trigger coverage up to $|\eta| = 4.0$ [22].

A two-level trigger system will be used to select events, reducing the event rate to about 10 kHz. In the reference scenario, the bandwidth allocated to di-lepton ($ee$, $\mu\mu$, $e\mu$) triggers is expected to be 0.2 kHz per trigger, where an offline selection of $p_{\mathrm{T}} > 10$ GeV for each lepton ensures full efficiency. For the missing transverse energy ($E_{\mathrm{T}}^{\mathrm{miss}}$) trigger, the bandwidth allocated is $\sim 0.4$ kHz, with $> 210$ GeV representing the offline $E_{\mathrm{T}}^{\mathrm{miss}}$ above which a typical analysis would use the data according to the Technical Design Report for the Phase-II upgrade of the ATLAS TDAQ system [25].

## 4 Monte Carlo Samples

Monte Carlo (MC) simulated event samples are used to predict the background from SM processes and to model the dark matter signal. The most relevant MC samples have equivalent luminosities (at 14 TeV) of at least 3000 fb$^{-1}$. The technical implementation of these samples is summarised in Table 1, including the packages used to perform matrix element generation and parton showering. The order at which the cross-section is computed for a given process is also shown, along with the specific choice of Parton Distribution Function (PDF) and tune. The dark-matter $t\bar{t}$ and $b\bar{b}$ signal samples are generated following the prescriptions in Ref. [15] and the $Wt$ signal samples ($Wt + \phi/a$) are generated following Ref [19]. For the $Wt + \phi/a$ model the production cross-section is computed at leading-order (LO) accuracy in the strong coupling constant $\alpha_{\mathrm{S}}$. For the $t\bar{t} + \phi/a$ and $b\bar{b} + \phi/a$ models the production cross-section is computed at next-to-LO (NLO) accuracy. Lastly, the $Z/\gamma^*$+jets and $W$+jets samples are generated with $\sqrt{s} = 13$ TeV. A collision energy of 14 TeV is replicated by applying an event weight based on the momentum fraction carried by the colliding partons and the ratio of PDF distributions for the different beam energies.

To emulate the Phase-II run conditions and detector response, the signal and SM background samples are smeared using performance functions derived from MC events passed through a full GEANT 4 simulation of the upgraded ATLAS detector [28–30]. Specifically, smearing is applied to the resolution and reconstruction efficiencies of the physics objects discussed in Section 5 using parameterisations made with $\langle\mu\rangle = 200$. The contribution from pileup is emulated by overlaying jets from a dedicated library.

Table 1: Summary of the simulated signal and SM background event samples used in this analysis, including the event generator, parton shower package, cross-section normalisation, PDF set, and underlying event parameter tune.

| Physics process | Generator | Parton shower | Cross-section normalisation | PDF set | Tune |
|---|---|---|---|---|---|
| $t\bar{t}+\phi/a$ Signal<br>$b\bar{b}+\phi/a$ Signal | aMC@NLO 2.3.3 | Pythia 8.212 | NLO | NNPDF30NLO | A14 [31] |
| $Wt+\phi/a$ Signal | aMC@NLO 2.4.3 | Pythia 8.212 | LO | NNPDF23LO | A14 |
| $t\bar{t}$ | Powheg-Box v2 [32–34] | Pythia 8.186 [35] | NNLO | NNLO CT10 [36] | A14 |
| Single-top ($t$-channel) | powheg-box v1 | Pythia 6.428 | NNLO+NNLL [37] | NLO CT10f4 | Perugia2012 |
| Single-top ($s$- and $Wt$-channel) | powheg-box v2 | Pythia 6.428 | NNLO+NNLL [38, 39] | NLO CT10 | Perugia2012 |
| $t\bar{t}W/Z/\gamma^*$ | aMC@NLO 2.2.2 | Pythia 8.186 | NLO [40] | NNPDF2.3LO | A14 |
| Diboson | Sherpa 2.2.1 [41] | Sherpa 2.2.1 | Generator NLO | CT10 [36] | Sherpa default |
| $t\bar{t}h$ | aMC@NLO 2.2.2 | Herwig 2.7.1 [42] | NLO [43] | CTEQ6L1 [44] | A14 |
| $Wh$, $Zh$ | aMC@NLO 2.2.2 | Pythia 8.186 | NLO [43] | NNPDF2.3LO | A14 |
| $t\bar{t}WW$, $t\bar{t}t\bar{t}$ | aMC@NLO 2.2.2 | Pythia 8.186 | NLO [40] | NNPDF2.3LO | A14 |
| $tZ$, $tWZ$, $t\bar{t}t$ | aMC@NLO 2.2.2 | Pythia 8.186 | LO | NNPDF2.3LO | A14 |
| Triboson | Sherpa 2.2.1 | Sherpa 2.2.1 | Generator LO, NLO | CT10 | Sherpa default |
| $Z/\gamma^*$+jets | Sherpa 2.2.1 [45] | Sherpa 2.2.1 [45] | NNLO [46] | NLO CT10 [36] | Sherpa default |
| $W$+jets | Sherpa 2.2.1 [45] | Sherpa 2.2.1 [45] | NNLO [46] | NLO CT10 [36] | Sherpa default |

# 5 Final State Object Selections

Selecting events consistent with the production of dark matter in a final state with either bottom or top quarks requires the reconstruction of jets, muons, electrons, and missing transverse momentum, $\vec{p}_{\mathrm{T}}^{\,\mathrm{miss}}$, where $E_{\mathrm{T}}^{\mathrm{miss}} = |\vec{p}_{\mathrm{T}}^{\,\mathrm{miss}}|$. This section describes the object definitions and kinematic variables used to discriminate signal from SM background processes in the two search channels.

In the previous search, $\vec{p}_{\mathrm{T}}^{\,\mathrm{miss}}$ is calculated as the negative vector sum of the transverse momenta of all identified physics objects [13]. A soft term constructed from all tracks unmatched to any physics object and originating from the primary vertex is also added. For the studies performed in this note however, the $\vec{p}_{\mathrm{T}}^{\,\mathrm{miss}}$ is computed at generator-level as the vectorial sum of the momenta of all neutral weakly-interacting particles in an event, including neutrinos and the dark matter candidate. This quantity is then smeared based on the $\vec{p}_{\mathrm{T}}^{\,\mathrm{miss}}$ resolution associated with the smeared sum of energies of interacting particles in the event.

Jet candidates are reconstructed using the anti-k$_t$ jet clustering algorithm with a radius parameter R = 0.4 [47] and are required to have transverse momentum $p_{\mathrm{T}} > 20$ GeV and $|\eta| < 3.8$. Tracking confirmation is applied to all jets to reduce the contribution from particle decays originating from pile-up interactions [48].

Decays from $b$-quarks are identified ($b$-tagged) using parametrisations that model the performance of the Run-2 multivariate $b$-tagging algorithm MV2c10 [49–51] as a function of jet $p_{\mathrm{T}}$ and $\eta$. Candidate $b$-jets must pass an identification requirement corresponding to an efficiency of 70% for jets containing $b$-hadrons in simulated $t\bar{t}$ events. This requirement represents the tightest set of restrictions on $b$-jets for

which flavour-tagging performance functions are available. The corresponding rejection factor for jets originating from the fragmentation of a c (light) quark is ~20 (750) [26].

Baseline electron candidates with $p_{\mathrm{T}} > 7$ GeV are reconstructed in the region $|\eta| < 4.0$ and required to pass the "loose" likelihood-based identification requirements [52, 53]. Similarly, muon candidates with $p_{\mathrm{T}} > 6$ GeV and $|\eta| < 2.7$ are required to pass the "medium" identification criteria [54, 55]. Signal leptons in the DM+$t\bar{t}/Wt$ channels are further required to have $p_{\mathrm{T}} > 20$ GeV, to ensure constant trigger efficiencies in the relevant phase, and $|\eta| < 2.47$ (2.5) for electrons (muons). The reduced pseudorapidity range compared with the DM+$b\bar{b}$ channel is motivated by the topologies of DM+$t\bar{t}/Wt$ events, which are characterised by central leptons.

To resolve reconstruction ambiguities, an overlap removal algorithm is applied to baseline leptons and jets. Where a baseline electron is found to lie within $\Delta R = \sqrt{\Delta\phi^2 + \Delta\eta^2} = 0.2$ of a candidate jet, the jet is removed if it fails to pass $b$-jet identification criteria corresponding to an efficiency of 85%. The same is applied to jets in the DM+$b\bar{b}$ (DM+$t\bar{t}/Wt$) channel which lie within $\Delta R = 0.2$ (0.4) of a selected muon and which are not true $b$-jets. To avoid rejecting events featuring leptonic $c$- or $b$-hadron decays, electrons (muons) are discarded if they are found within a cone of $\Delta R = 0.4$ ($\Delta R = \max(0.4, 0.04 + (10\ \mathrm{GeV})/\mathrm{p}_T^{\mu})$) of any surviving jet.

## 6 Signatures with $b$-quarks and $E_{\mathrm{T}}^{\mathrm{miss}}$

To isolate the event topology of the DM+$b\bar{b}$ final state, events are required to have at least two $b$-tagged jets. The contribution from SM background processes is suppressed via the application selection criteria based on that of the 13 TeV analysis and updated to align with HL–LHC design considerations.

To reduce the contribution from leptonic and semi-leptonic $t\bar{t}$ decays and from leptonic decays of W and Z bosons, events containing at least one baseline lepton ($N_l^B$) are vetoed. A further requirement of no more than 2 or 3 jets is imposed in order to control the large background from hadronic $t\bar{t}$ decays which are typically characterised by high jet multiplicities. A minimum requirement on the azimuthal separation between each jet, $j$, and the missing transverse momentum, $\Delta\phi(j, \vec{p}_{\mathrm{T}}^{\mathrm{miss}}) > 0.4$, is also imposed in accordance with the treatment used at 13 TeV to suppress fake $E_{\mathrm{T}}^{\mathrm{miss}}$ in multi-jet events.

To reduce the contribution from the dominant Z+jets background, several variables exploiting the difference in spin between the scalar and pseudoscalar particles and the Z boson are defined. These variables make use of the pseudorapidity and azimuthal separations between jets, $b$-jets and the missing transverse momentum and include:

- The azimuthal correlation variables:

$$\delta^{-} = \Delta\phi(j, \vec{p}_{\mathrm{T}}^{\mathrm{miss}}) - \Delta\phi(b, b)$$
$$\delta^{+} = |\Delta\phi(j, \vec{p}_{\mathrm{T}}^{\mathrm{miss}}) + \Delta\phi(b, b) - \pi|$$

  where $\Delta\phi(j, \vec{p}_{\mathrm{T}}^{\mathrm{miss}}) = \phi(j) - \phi(\vec{p}_{\mathrm{T}}^{\mathrm{miss}})$ is the azimuthal separation between any jet in an event and $\vec{p}_{\mathrm{T}}^{\mathrm{miss}}$, and $\Delta\phi(b, b) = \phi(b_1) - \phi(b_2)$ is the azimuthal separation between the leading $b$-jet ($b_1$) and sub-leading $b$-jet ($b_2$).

- The momentum imbalance between the leading and sub-leading $b$-jets:

$$\text{Imb}(b,b) = \frac{p_T(b_1) - p_T(b_2)}{p_T(b_1) + p_T(b_2)}$$

- The cosine of $\pi - \Delta\phi(b,b)$:

$$\cos(\pi - \Delta\phi(b,b))$$

- The hyperbolic tangent of the pseudorapidity separation between the leading and sub-leading $b$-jet, $\Delta\eta(b,b) = \eta(b_1) - \eta(b_2)$:

$$\cos\theta^*_{bb} = \left|\tanh\left(\frac{|\Delta\eta(b,b)|}{2}\right)\right|$$

$b$-jets produced in association with vector particles are expected to yield a reasonably flat $\cos\theta^*_{bb}$ distribution. For $b$-jets accompanying the production of a heavy scalar or pseudoscalar mediator however, $\cos\theta^*_{bb}$ is expected to peak around 1. The distribution of this variable, along with those of other key discriminants, is shown in Figure 2.

To reduce the contribution from processes where spin anti-correlations are not present or easily exploited, events are required to pass a cut on $H_{\text{T}}^{\text{ratio}}$, the ratio of the leading jet transverse momentum, $p_T(j_1)$, to the scalar sum of the transverse momenta of all jets in the event, $H_{\text{T}}$. Also used is the hyperbolic tangent of the $\eta$ separation between the leading ($j_1$) and third-leading jet ($j_3$):

$$\cos\theta^*_{j_1 j_3} = \left|\tanh\left(\frac{\Delta\eta(j_1,j_3)}{2}\right)\right|$$

In signal events with 3 jets the first and third jet are largely produced back-to-back, leading to a peak at approximately 1 in the $\cos\theta^*_{j_1 j_3}$ distribution. In contrast, $j_1$ and $j_3$ in events from SM background processes – in particular, from $t\bar{t}$ decays – exhibit strong collinearity, leading to dominance in the region below 0.5 as shown in Figure 2(b). Note that a cut on $\cos\theta^*_{j_1 j_3}$ is only applied to events with 3 jets.

As seen from Figure 2(c), the shape of the $\cos\theta^*_{bb}$ distribution for the scalar and pseudoscalar signals can depend strongly on the mass of the mediating particle. Consequently, separate selections are derived for $m(\phi/a) < 100$ GeV and $m(\phi/a) \geq 100$ GeV. The resulting signal regions, denoted by $\text{SR}_{b,\text{low}}$ and $\text{SR}_{b,\text{high}}$ respectively, are defined in Table 2.

The $\cos\theta^*_{bb}$ variable provides the best discrimination between signal and background events. As such, $\text{SR}_{b,\text{low}}$ and $\text{SR}_{b,\text{high}}$ are divided into four equal-width exclusive bins in $\cos\theta^*_{bb}$, reflecting the configuration used in Run 2. The bins are denoted by the labels $\text{SR}_{b,X}$-bin1 through $\text{SR}_{b,X}$-bin4 where $X = \{\text{low}, \text{high}\}$.

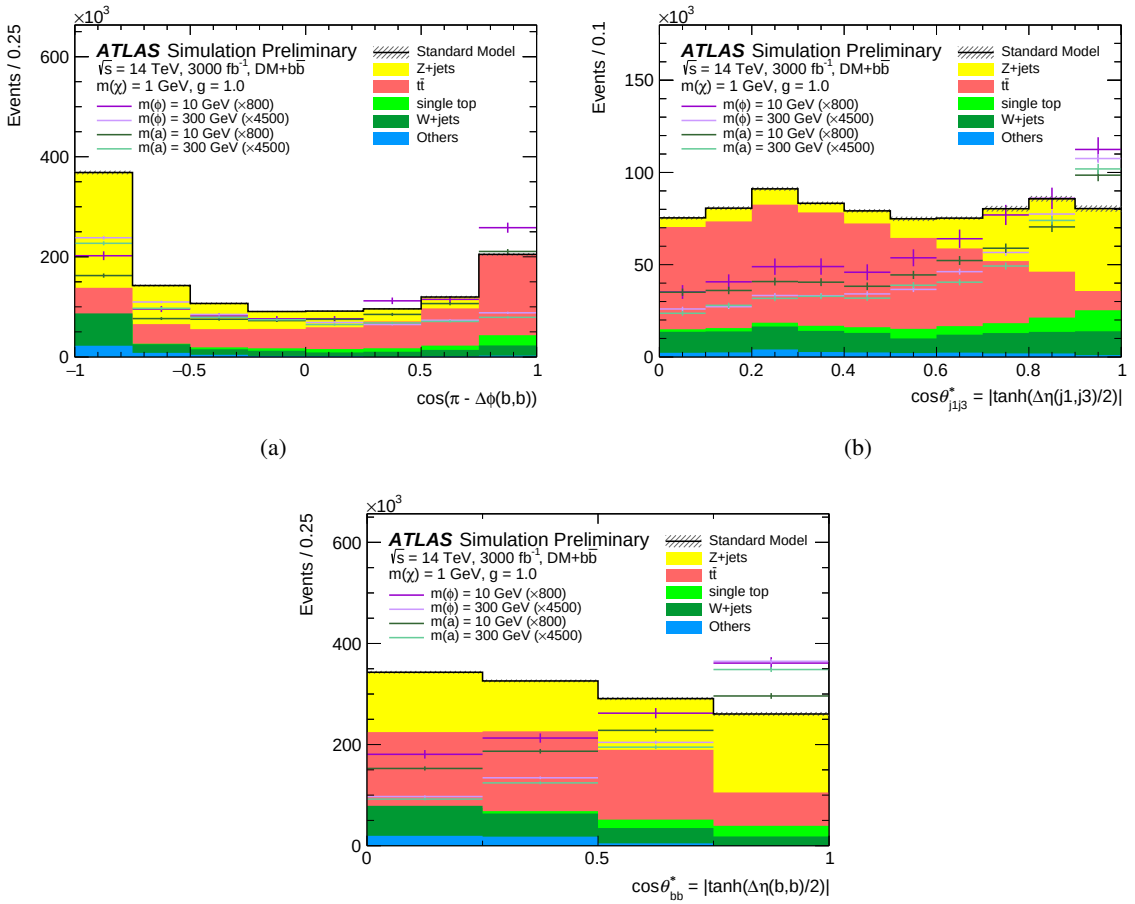


(a) (b)

(c)

Figure 2: Distributions of several key discriminants in the DM+$b\bar{b}$ analysis following the requirement of $E_{\mathrm{T}}^{\mathrm{miss}}$ >210 GeV, no leptons, 2 or 3 jets, and at least two identified $b$-jets. The hatched bands and error bars represent the statistical uncertainty on the total SM background and signal yields respectively.

# 7 Signatures with top quarks and $E_{\mathrm{T}}^{\mathrm{miss}}$

In order to target dark matter produced in association with one (DM+$Wt$) or two (DM+$t\bar{t}$) top quarks, one signal region is defined, and it is denoted denoted $\mathrm{SR}_{2\ell}$. Events are required to have exactly two opposite electric charge leptons, electrons or muons, either same- or different-flavour with an invariant mass (regardless of the flavours of the leptons in the pair), $m_{\ell\ell}$, being larger than 100 GeV in order to reduce the $t\bar{t}$ background. Furthermore, candidate signal events are required to have at least one identified $b$-jet. Different discriminators and kinematic variables have been used to further separate the $t\bar{t}+\phi/a$ and $Wt+\phi/a$ signal from the SM background.

- $m_{b2\ell}^{\mathrm{min}}$ is the smallest invariant mass computed between the leading $p_{\mathrm{T}}$ $b$-tagged jet and each of the two leptons in the event. In events with two top quarks decaying dileptonically, at least one of the two mass combinations must be bounded from above by $m_{b2\ell}^{\mathrm{min}} < \sqrt{m_t^2 - m_W^2}$.

- $\mathbf{p}_{\mathrm{T,boost}}^{\ell\ell}$: defined as the vector

$$\mathbf{p}^{\ell\ell}_{\mathrm{T,boost}} = \mathbf{p}^{\mathrm{miss}}_{\mathrm{T}} + \mathbf{p}_{\mathrm{T}}(\ell_1) + \mathbf{p}_{\mathrm{T}}(\ell_2).$$

The $\mathbf{p}^{\ell\ell}_{\mathrm{T,boost}}$ variable, with magnitude $p^{\ell\ell}_{\mathrm{T,boost}}$, can be interpreted as the opposite of the vector sum of all the transverse hadronic activity in the event.

- $\Delta\phi_{\mathrm{boost}}$: the azimuthal angle between the $\mathbf{p}^{\mathrm{miss}}_{\mathrm{T}}$ vector and the $\mathbf{p}^{\ell\ell}_{\mathrm{T,boost}}$ vector [56].
- $m_{\mathrm{T2}}$: lepton-based stransverse mass. The stransverse mass [57, 58] is a kinematic variable used to bound the masses of a pair of intermediate particles which are presumed to each have decayed semi-invisibly into one visible and one invisible particle. The stransverse mass is defined as

$$m_{\mathrm{T2}}(\mathbf{p}_{\mathrm{T},1}, \mathbf{p}_{\mathrm{T},2}, \mathbf{q}_{\mathrm{T}}) = \min_{\mathbf{q}_{\mathrm{T},1}+\mathbf{q}_{\mathrm{T},2}=\mathbf{q}_{\mathrm{T}}} \left\{ \max[\, m_{\mathrm{T}}(\mathbf{p}_{\mathrm{T},1}, \mathbf{q}_{\mathrm{T},1}), m_{\mathrm{T}}(\mathbf{p}_{\mathrm{T},2}, \mathbf{q}_{\mathrm{T},2}) \,] \right\},$$

  where $m_{\mathrm{T}}$ indicates the transverse mass[2], $\mathbf{p}_{\mathrm{T},1}$ and $\mathbf{p}_{\mathrm{T},2}$ are the transverse momentum vectors of the two particles (assumed to be massless), and $\mathbf{q}_{\mathrm{T},1}$ and $\mathbf{q}_{\mathrm{T},2}$ are the unknown transverse momentum vectors of the invisible particles, with $\mathbf{q}_{\mathrm{T}} = \mathbf{q}_{\mathrm{T},1} + \mathbf{q}_{\mathrm{T},2}$. The minimisation is performed over all the possible decompositions of $\mathbf{q}_{\mathrm{T}}$. For $t\bar{t}$ or $WW$ events, where the transverse momenta of the two leptons in each event are taken as $\mathbf{p}_{\mathrm{T},1}$ and $\mathbf{p}_{\mathrm{T},2}$, and $p^{\mathrm{miss}}_{\mathrm{T}}$ as $\mathbf{q}_{\mathrm{T}}$, $m_{\mathrm{T2}}(\ell_1, \ell_2, E^{\mathrm{miss}}_{\mathrm{T}})$ is bounded sharply from above by the mass of the $W$ boson [59, 60], while signal events do not respect this bound because of the additional $E^{\mathrm{miss}}_{\mathrm{T}}$ coming from the undetected DM particles.

A summary of the analysis selections of $\mathrm{SR}_{2\ell}$ is presented in Table 2. For reference, the distribution of the $m_{\mathrm{T2}}$ variable for events passing all of the $\mathrm{SR}_{2\ell}$ requirements except that on $m_{\mathrm{T2}}$ is shown in Figure 3.

For the exclusion limits presented in Section 9, the $m_{\mathrm{T2}}$ distribution is divided into five exclusive bins between ([200,220],[220,240],[240,260],[260,280],[>280]) GeV following an approach similar to that used for $\mathrm{SR}_{b,\mathrm{low}}$ and $\mathrm{SR}_{b,\mathrm{high}}$. The bins are denoted by the labels $\mathrm{SR}_{2\ell}$-bin1 through $\mathrm{SR}_{2\ell}$-bin5 and span the range of $m_{\mathrm{T2}}$ between 200 GeV and 300 GeV. The last bin also includes events with $m_{\mathrm{T2}} > 300$ GeV.

[2] The transverse mass is defined as $m_{\mathrm{T}} = \sqrt{2|\mathbf{p}_{\mathrm{T},1}||\mathbf{p}_{\mathrm{T},2}|(1-\cos(\Delta\phi))}$, where $\Delta\phi$ is the angle between the particles with transverse momenta $\mathbf{p}_{\mathrm{T},1}$ and $\mathbf{p}_{\mathrm{T},2}$ in the plane perpendicular to the beam axis.

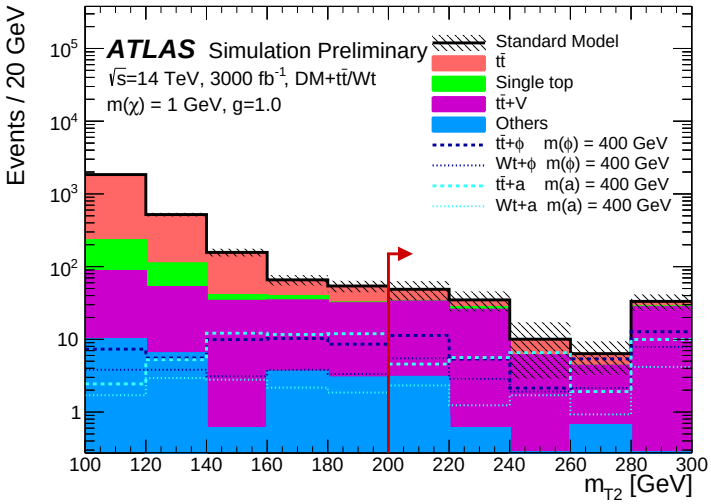


Figure 3: Distribution of $m_{\mathrm{T2}}$ for events satisfying the SR criteria except that on $m_{\mathrm{T2}}$. The contributions from all SM backgrounds are shown; the hatched bands represent the systematic uncertainty. The rightmost bin includes overflow events.

Table 2: Summary of the analysis selection criteria (see text for details).

| | $\mathrm{SR}_{b,\mathrm{low}}$ | $\mathrm{SR}_{b,\mathrm{high}}$ | $\mathrm{SR}_{2\ell}$ |
|---|---|---|---|
| $N_\ell$ | 0 | 0 | 2 |
| $N_{\mathrm{jets}}$ | 2 or 3 | 2 or 3 | $\geq 1$ |
| $N_{b\text{-jets}}$ | $\geq 2$ | $\geq 2$ | $\geq 1$ |
| $\lvert\eta_j\rvert$ | $< 3.0$ | $< 3.8$ | $< 2.5$ |
| $m_{\ell\ell}$ | - | - | $> 100$ GeV |
| $E_{\mathrm{T}}^{\mathrm{miss}}$ | $> 210$ GeV | $> 300$ GeV | $> 300$ GeV |
| $m_{b2\ell}^{\mathrm{min}}$ | - | - | $< 150$ GeV |
| $\Delta\phi_{\mathrm{boost}}$ | - | - | $< 1.5$ |
| $p_T(j_1)$ | $> 130$ GeV | $> 200$ GeV | $> 100$ GeV |
| $p_T(j_3)$ | $< 50$ GeV | $< 90$ GeV | - |
| $H_{\mathrm{T}}^{\mathrm{ratio}}$ | $> 0.75$ | $> 0.4$ | - |
| $\delta^-$ [rad] | - | $< 0.5$ | - |
| $\delta^+$ [rad] | - | $< 1.0$ | - |
| Imb($b$,$b$) | - | $< 0.6$ | - |
| $\cos(\pi - \Delta\phi(b,b))$ | $> 0.75$ | - | - |
| $\cos\theta^*_{j_1 j_3}$ | $> 0.8$ | $> 0.75$ | - |
| $m_{\mathrm{T2}}$ | - | - | $> 200$ GeV |

## 8 Systematic Uncertainties

Systematic uncertainties based on those in Ref. [13] are applied to signal and SM background processes. The uncertainties are scaled to align with HL–LHC extrapolations developed by the ATLAS and CMS Collaborations and documented in Ref. [30]. During Phase-II operation, the theory modelling uncertainties are expected to halve, while the degree of reduction of experimental uncertainties like, for example, the jet energy scale and $b$-jet mis-identification depend on the signal region. This results in a total expected systematic uncertainty on the SM background of 13.42% for $\mathrm{SR}_{b,\mathrm{low}}$/$\mathrm{SR}_{b,\mathrm{high}}$ and 13% for $\mathrm{SR}_{2\ell}$, corresponding to a reduction of ∼15% and ∼54% respectively compared to the 13 TeV analysis. Statistical uncertainties due to the limited size of the Monte Carlo samples used for the modelling of signal and SM background processes are neglected.

Two types of hypothesis tests are performed in order to extract expected discovery $p$-values and 95% CL exclusion limits. For the $p$-values, a cut-and-count experiment is employed assuming uncertainty only on the SM background yield. The value of this uncertainty is set to the total background uncertainty reported above. For the exclusion limits, the sensitivity is evaluated by performing a profile-likelihood fit to pseudo-data corresponding to the expected background and signal yields in each multi-bin signal region. The likelihood is built as the product of Poissonian terms, one for each of the bins considered. Systematic uncertainties are incorporated as Gaussian distributed nuisance parameters affecting both the overall normalisation of the fit variable and the individual bin yields. For the former, the uncertainty on the SM background contribution is modelled by a nuisance parameter with value equal to the total background uncertainty. For the signal contribution, experimental uncertainty is accounted for by a nuisance parameter with a value of 10% (9.4%) for $\mathrm{SR}_{b,\mathrm{low}}$/$\mathrm{SR}_{b,\mathrm{high}}$ ($\mathrm{SR}_{2\ell}$), corresponding to the HL–LHC extrapolation of the Run 2 detector- and reconstruction-based uncertainties. A separate nuisance parameter with a value of 5% is also included to account for theoretical uncertainties on the signal models. The nuisance parameters affecting the individual bin yields account for potential inaccuracies in the extrapolated theory and experimental uncertainties. Such inaccuracies may result from, for example, the difference in selection criteria between a HL–LHC search and the reference Run 2 search.

## 9 Results

The predicted yields in the $\mathrm{SR}_{b,\mathrm{low}}$, $\mathrm{SR}_{b,\mathrm{high}}$ and $\mathrm{SR}_{2\ell}$ signal regions are reported in Tables 3, 4 and 5 respectively. For both $\mathrm{SR}_{b,\mathrm{low}}$ and $\mathrm{SR}_{b,\mathrm{high}}$, the main background consists of $Z/\gamma^*$+jets events followed by hadronic decays of $t\bar{t}$. A significant contribution also comes from single top quark processes and events featuring a $W$-boson produced in association with jets ("$W$+jets"). Note that the minor background from di-boson, tri-boson, and $t\bar{t}+Z/W$ , $t\bar{t}+WW/ZZ/WZ$ processes in $\mathrm{SR}_{b,\mathrm{low}}$ and $\mathrm{SR}_{b,\mathrm{high}}$ is referred to collectively as "Others".

In $\mathrm{SR}_{2\ell}$, the dominant background consists of di-leptonic decays of $t\bar{t}$ and $t\bar{t}Z$ with $Z \to \nu\nu$. As with $\mathrm{SR}_{b,\mathrm{low}}$ and $\mathrm{SR}_{b,\mathrm{high}}$, the SM processes that make a minor contribution are merged into an "Others" category. In $\mathrm{SR}_{2\ell}$, this category contains the background from di-/tri-boson, $Z/\gamma^*$+jets, $t\bar{t}\,t\bar{t}$, and $t\bar{t}+WW$ processes.

| | $SR_{b,low}$-bin1 | $SR_{b,low}$-bin2 | $SR_{b,low}$-bin3 | $SR_{b,low}$-bin4 |
|---|---|---|---|---|
| SM events | 2542 ± 75 | 2436 ± 92 | 2861 ± 103 | 2585 ± 138 |
| $Z/\gamma^*$+jets events | 1337 ± 64 | 1410 ± 82 | 1885 ± 96 | 2030 ± 136 |
| $t\bar{t}$ events | 785 ± 37 | 708 ± 41 | 685 ± 35 | 384 ± 26 |
| Single top quark events | 166.8 ± 8.0 | 137.6 ± 8.0 | 143.8 ± 7.3 | 146.0 ± 9.8 |
| W+jets events | 252.9 ± 12.1 | 151.0 ± 8.8 | 108.1 ± 5.5 | 24.7 ± 1.7 |
| Others events | 0.81 ± 0.04 | 28.2 ± 1.6 | 39.1 ± 2.0 | −− |
| $b\bar{b} + \phi$ (10 GeV) | 12.21 ± 0.83 | 11.43 ± 0.86 | 14.55 ± 0.98 | 15.0 ± 1.2 |
| $b\bar{b} + a$ (10 GeV) | 10.48 ± 0.50 | 14.62 ± 0.85 | 14.73 ± 0.75 | 13.11 ± 0.88 |

Table 3: Expected yields in $SR_{b,low}$ for SM background processes and a selection of signal masses for an integrated luminosity of 3000 fb$^{-1}$at $\sqrt{s}$ = 14 TeV. The uncertainties on the quoted numbers correspond to the MC statistical uncertainty.

| | $SR_{b,high}$-bin1 | $SR_{b,high}$-bin2 | $SR_{b,high}$-bin3 | $SR_{b,high}$-bin4 |
|---|---|---|---|---|
| SM events | 1130 ± 54 | 1208 ± 47 | 1218 ± 52 | 1054 ± 52 |
| $Z/\gamma^*$+jets events | 572 ± 45 | 594 ± 39 | 665 ± 46 | 698 ± 49 |
| $t\bar{t}$ events | 346 ± 27 | 343 ± 23 | 312 ± 22 | 214 ± 15 |
| Single top quark events | 101.4 ± 8.0 | 110.3 ± 7.3 | 108.2 ± 7.5 | 101.6 ± 7.1 |
| $W$+jets events | 40.4 ± 3.2 | 108.1 ± 7.1 | 104.6 ± 7.2 | 40.1 ± 2.8 |
| Others events | 69.8 ± 5.5 | 53.2 ± 3.5 | 28.2 ± 2.0 | −− |
| $b\bar{b} + \phi$ (300 GeV) | 0.70 ± 0.05 | 0.76 ± 0.045 | 0.92 ± 0.06 | 1.22 ± 0.07 |
| $b\bar{b} + a$ (300 GeV) | 0.51 ± 0.04 | 0.68 ± 0.04 | 0.66 ± 0.05 | 0.94 ± 0.07 |

Table 4: Expected yields in $SR_{b,high}$ for SM background processes and a selection of signal masses for an integrated luminosity of 3000 fb$^{-1}$at $\sqrt{s}$ = 14 TeV. The uncertainties on the quoted numbers correspond to the MC statistical uncertainty.

The results are translated into constraints on the scalar and pseudoscalar models using the HistFitter package [61], which employs a profile-likelihood-ratio test statistic to perform hypothesis testing [62]. The package is used to compute the expected discovery $p$-values for the scalar and pseudoscalar mediator models. For a flavour-universal coupling between $\phi/a$ and the SM quarks, only $SR_{2\ell}$ is sensitive to dark matter production. Scans of the expected discovery significance in this signal region are shown in Figure 4 as a function of the mediator mass. The $5\sigma$ discovery potential for the full HL–LHC dataset is expected to extend up to $m(\phi)$ = 105 GeV and $m(a)$ = 150 GeV for the DM+$t\bar{t}$ channel. Addition of the DM+$Wt$ channel further extends the discovery potential to $m(\phi)$ = 155 GeV and $m(a)$ = 250 GeV.

The HistFitter package is also used to compute the expected exclusion limits for each model with the $CL_s$ prescription [63] and assuming no excess in the observed data. The limits are shown in Figures 5 and 6 for $\phi/a \rightarrow \chi\bar{\chi}$ production in association with bottom quarks and top quarks respectively for $\mathcal{L}$ = 3000 fb$^{-1}$ at $\sqrt{s}$ = 14 TeV. The contours correspond to the 95% CL upper limit on the ratio of the measurable cross-section with respect to the theoretically predicted cross-section for $g$ = 1.0. Also shown for comparison are the corresponding limits at $\sqrt{s}$ = 13 TeV with 36.1 fb$^{-1}$ of data [13].

For the DM+$b\bar{b}$ channel, cross-sections ∼45–100 times the theoretically predicted for $g$ = 1.0 and

| | $SR_{2\ell}$ | $SR_{2\ell}$-bin1 | $SR_{2\ell}$-bin2 | $SR_{2\ell}$-bin3 | $SR_{2\ell}$-bin4 | $SR_{2\ell}$-bin5 |
|---|---|---|---|---|---|---|
| | 133 ± 21 | 49 ± 14 | 35 ± 10 | 10.0 ± 7.1 | 6.4 ± 3.0 | 33.3 ± 8.3 |
| $t\bar{t}$ events | 33.3 ± 5.3 | 15.1 ± 4.5 | 7.1 ± 2.2 | 4.05 ± 2.9 | 2.0 ± 1.0 | 5.0 ± 1.3 |
| $t\bar{t}$ +$V$ events | 92 ± 15 | 29.9 ± 8.8 | 24.9 ± 7.7 | 6.00 ± 4.3 | 3.7 ± 1.8 | 27.4 ± 6.7 |
| Single top quark events | 3.82 ± 0.61 | 0.76 ± 0.23 | 2.30 ± 0.70 | −− | −− | 0.76 ± 0.20 |
| Others events | 4.30 ± 0.43 | 3.00 ± 0.70 | 0.60 ± 0.18 | −− | 0.66 ± 0.32 | −− |
| $t\bar{t}/Wt + a$ (50 GeV) | 235 ± 18 | 62.9 ± 9.6 | 42.6 ± 7.3 | 45.1 ± 8.6 | 19.6 ± 4.3 | 64.5 ± 8.1 |
| $t\bar{t}/Wt + \phi$ (50 GeV) | 219 ± 33 | 61 ± 17 | 58 ± 16 | 10.6 ± 4.4 | 17.0 ± 9.8 | 71 ± 22 |
| $t\bar{t}/Wt + a$ (400 GeV) | 39.0 ± 4.9 | 6.9 ± 1.8 | 6.8 ± 1.8 | 8.3 ± 3.3 | 2.8 ± 1.0 | 14.1 ± 2.6 |
| $t\bar{t}/Wt + \phi$ (400 GeV) | 57.2 ± 6.6 | 16.8 ± 3.7 | 8.2 ± 2.0 | 4.0 ± 2.0 | 7.5 ± 2.0 | 20.6 ± 3.4 |

Table 5: Expected yields in $SR_{2\ell}$ for SM background processes and a selection of signal masses for an integrated luminosity of 3000 fb$^{-1}$at $\sqrt{s}$ = 14 TeV. The uncertainties on the quoted numbers correspond to the MC statistical uncertainty.

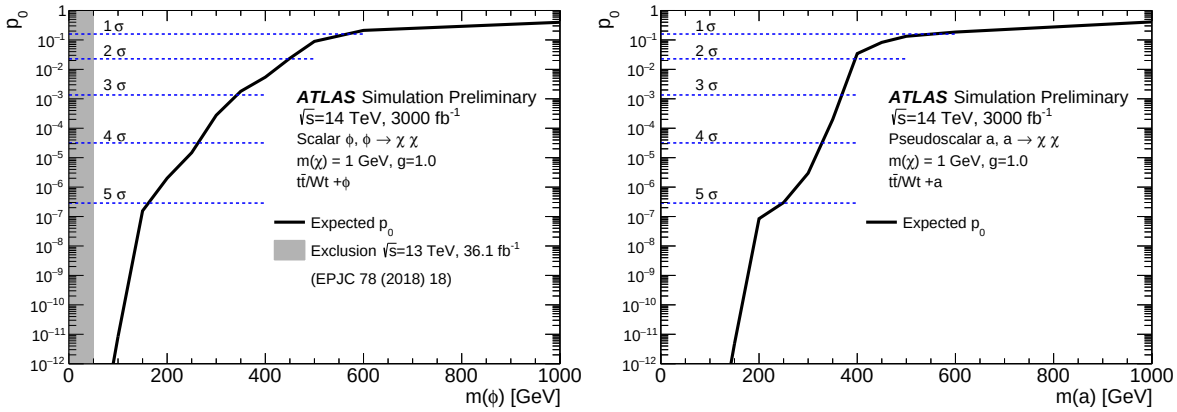


(a) (b)

Figure 4: Expected compatibility, represented by the $p$-value $p_0$, of the background-only hypothesis with the production of a colour-neutral (left) scalar or (right) pseudoscalar mediator in association with one or two top quarks for 3000 fb$^{-1}$ of 14 TeV proton-proton collision data. The compatibility is given as a function of the mediator mass assuming $\phi/a \to \chi\bar{\chi}$ and $g$ = 1.0.

$m(\phi/a) < 100$ GeV are excluded with the anticipated HL–LHC dataset. This corresponds to a factor of 3–3.5 (3–4.3) improvement with respect to the previous reach achievable for the scalar (pseudoscalar) mediator model. Similarly, for $m(\phi/a) \geq 100$ GeV, the extended coverage in pseudorapidity afforded by the upgrade to the ATLAS Inner Tracker allows for better exploitation of anti-correlations in jet and $b$-jet spin-sensitive variables like $\cos\theta^*_{bb}$. This results in a larger gain in the exclusion potential for the high-mass region, equivalent to a factor of 5.8–8.7 (3–5) increase with respect to the 13 TeV limit for scalar (pseudoscalar) masses in the range 100–500 GeV.

As mentioned previously, the DM+$b\bar{b}$ channel is better motivated within the context of the 2HDM+$a$ model, offering appealing prospects for constraints on $\tan\beta$. Using the same 2HDM+$a$ model as in Ref. [18] and assuming a large mass splitting between the two pseudoscalar states ($A$ and $a$ with $m(A) >$

$m(a)$), an upper bound on $\tan\beta$ can be approximated by the formula [17]:

$$\tan\beta \simeq \left[\frac{g_\chi g_\nu}{y_\chi \sin\theta}\left(\frac{\sigma}{\sigma(g=1.0)}\right)\right]^{1/2} = \left[\frac{1}{y_\chi \sin\theta}\left(\frac{\sigma}{\sigma(g=1.0)}\right)\right]^{1/2}$$

where $\sigma/\sigma(g=1.0)$ corresponds to the value of the exclusion limit for $pp \to a + b\bar{b}$ in the context of the simplified pseudoscalar mediator model. For $\sin\theta = 0.35$ and $y_\chi = 1$ (a common choice of parameter values), expected bounds on $\tan\beta$ achievable at the HL–LHC range from ~19 for $m(a) = 10$ GeV to ~100 for $m(a) = 500$ GeV, significantly extending the current phase space coverage.

The exclusion limits in Figure 6 include the contributions from both the DM+$t\bar{t}$ and DM+$Wt$ final states. Considering only the DM+$t\bar{t}$ channel, the limit is expected to extend up to $m(\phi) = 405$ GeV and $m(a) = 385$ GeV. In the case of the scalar mediator model, this represents a factor of 5 improvement with respect to the 13 TeV result. The statistical precision of the signal models has been found to be the main limiting factor in assessing the sensitivity of the DM+$t\bar{t}$/$Wt$ channel. If a single-bin signal region defined by the inclusive selection ($SR_{2\ell}$) is considered in place of the multi-bin selection, the exclusion limits in Figure 6 are reduced by a maximum of 20%, with scalar mediator masses below 100 GeV predominantly affected. For reference, the statistical uncertainties on the signal and SM background yields are provided in Table 5. Statistical uncertainties are also provided for the DM+$b\bar{b}$ channel in Tables 3 and 4.

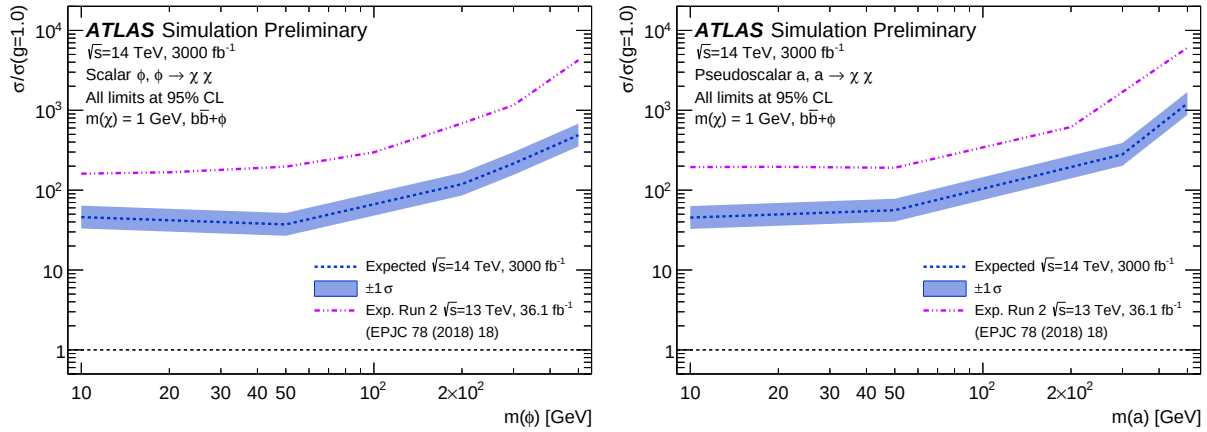


(a) (b)

Figure 5: Exclusion limits for the production of a colour-neutral (left) scalar or (right) pseudoscalar mediator in association with bottom quarks and decaying to a pair of dark matter particles with mass 1 GeV. The limits, calculated at 95% CL, are given as a function of the mediator mass and represent the ratio of the excluded cross-section to the theoretically predicted cross-section for a coupling, $g = 1.0$, and for 3000 fb$^{-1}$ of 14 TeV proton-proton collision data. The solid bands correspond to the expected limit $\pm 1\sigma$. Also shown for comparison is the expected limit for 36.1 fb$^{-1}$ of 13 TeV proton-proton collision data taken from the previous analysis [13] (pink).

For each dark matter and mediator mass pair, the exclusion limit on the production cross-section of colour-neutral scalar mediator particles can be converted into a limit on the spin-independent DM–nucleon scattering cross-section using the procedure described in Ref. [64]. Figure 7 shows the resulting constraints in the plane defined by the dark-matter mass and the scattering cross-section, which are derived considering only the contribution from the $t\bar{t} + \phi$ model. The maximum value of the DM–nucleon scattering cross-section shown in the plot corresponds to the value of the cross section for a mediator

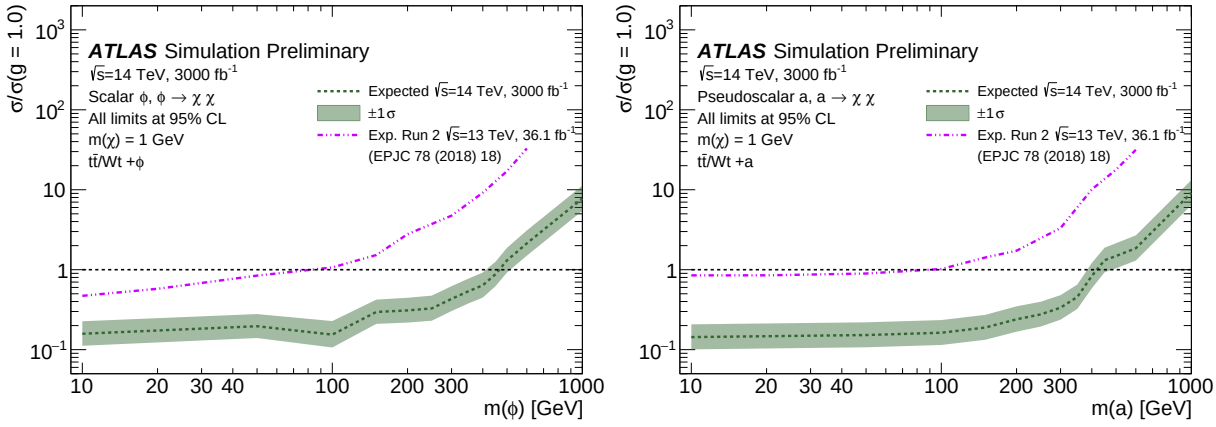


(a) (b)

Figure 6: Exclusion limits for the production of a colour-neutral (left) scalar or (right) pseudoscalar mediator in association with one or two top quarks and decaying to a pair of dark matter particles with mass 1 GeV. The limits, calculated at 95% CL, are given as a function of the mediator mass and represent the ratio of the excluded cross-section to the theoretically predicted cross-section for a coupling, $g = 1.0$, and for 3000 fb$^{-1}$ of 14 TeV proton-proton collision data. The solid bands correspond to the expected limit $\pm 1\sigma$. Also shown for comparison is the expected limit for 36.1 fb$^{-1}$ of 13 TeV proton-proton collision data taken from the previous analysis [13] (pink).

mass of 10 GeV. The red contour is the exclusion limit at 90% CL. The green contour indicates the $5\sigma$ discovery potential. The lower horizontal line in the green (red) contour corresponds to the value of the cross section for $m(\phi) = 105$ GeV ($m(\phi) = 430$ GeV). Overlaid for comparison are the most stringent direct detection limits to date from the LUX [65, 66], CRESST-III [67], XENON1T [68], PandaX [69] and DarkSide-50 [70] Collaborations.

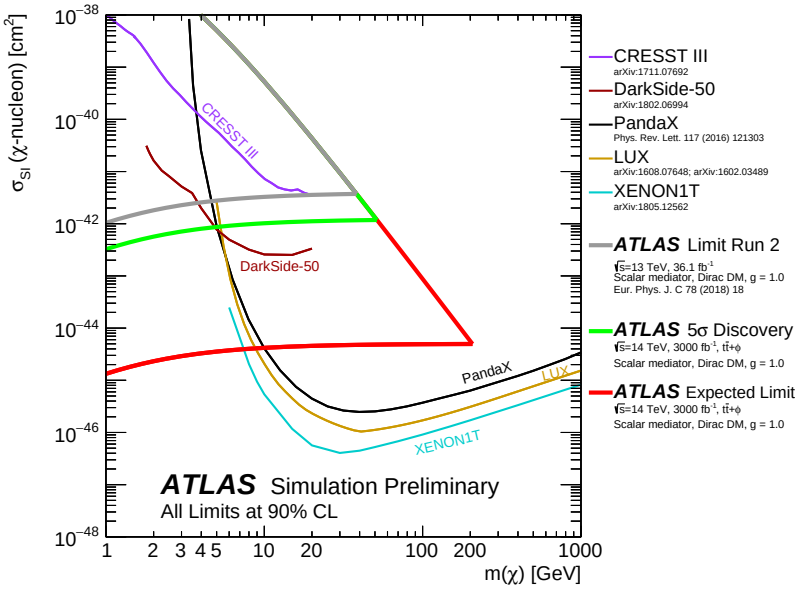


Figure 7: Comparison of the 90% CL limits on the spin-independent DM-nucleon cross-section as a function of DM mass between these results and the direct-detection experiments, in the context of the colour-neutral simplified model with scalar mediator. The green contour indicates the $5\sigma$ discovery potential at HL–LHC. The lower horizontal line of the DM–nucleon scattering cross-section for the red (green) contour corresponds to value of the cross section for $m(\phi) = 430$ GeV ($m(\phi) = 105$ GeV). The grey contour indicates the exclusion derived from the observed limits for 36.1 fb$^{-1}$ at 13 TeV taken from Ref. [13]. The results are compared with limits from direct detection experiments.

# 10 Conclusion

This note presents an estimate of the ATLAS sensitivity to dark matter production in association with heavy flavour quarks with 3000 fb$^{-1}$ of proton-proton collisions at $\sqrt{s} = 14$ TeV. Feasibility studies are carried out for two simplified models in which the dark and SM sectors are assumed to couple via the exchange of a spin-0 mediator. The studies are divided into two categories: dark matter production in association with a pair of bottom quarks, and dark matter production in association with one or two top quarks. Parametrisations derived from performance studies are used to emulate the response of the upgraded ATLAS detector with 200 interactions per bunch crossing. Exclusion limits are derived at 95% CL for mediator masses in the range 10–500 GeV assuming systematic uncertainties consistent with current forecasts. In comparison to results obtained with 36 fb$^{-1}$ in Run 2, the exclusion potential at the HL–LHC is found to improve by a factor of ~3–8.7 for scalar and pseudoscalar masses produced in association with bottom quarks, assuming unitary couplings and a dark matter mass of 1 GeV. In final states with one or two leptonically-decaying top quarks, the mass range for which a colour-neutral scalar mediator is expected to be excluded extends from 80 GeV to 405 GeV. Similarly, exclusion of pseudoscalar masses up to 385 GeV is expected.

## References


[1] E. Komatsu et al., *Seven-year Wilkinson Microwave Anisotropy Probe (WMAP) Observations: Cosmological Interpretation*, The Astrophysical Journal Supplement Series **192** (2011) 18.

[2] G. Bertone, D. Hooper and J. Silk, *Particle dark matter: Evidence, candidates and constraints*, Phys. Rept. **405** (2005) 279, arXiv: hep-ph/0404175 [hep-ph].

[3] G. Bertone and D. Hooper, *A History of Dark Matter*, Rev. Mod. Phys. **90** (2018) 045002, arXiv: 1605.04909 [astro-ph.CO].

[4] P. A. R. Ade et al., *Planck 2015 results. XIII. Cosmological parameters*, Astron. Astrophys. **594** (2016) A13, arXiv: 1502.01589 [astro-ph.CO].

[5] G. Steigman and M. S. Turner, *Cosmological Constraints on the Properties of Weakly Interacting Massive Particles*, Nucl. Phys. B **253** (1985) 375.

[6] CMS Collaboration, *Search for dark matter produced with an energetic jet or a hadronically decaying W or Z boson at* $\sqrt{s} = 13$ *TeV*, JHEP **07** (2017) 014, arXiv: 1703.01651 [hep-ex].

[7] CMS Collaboration, *Search for new physics in the monophoton final state in proton-proton collisions at* $\sqrt{s} = 13$ *TeV*, JHEP **10** (2017) 073, arXiv: 1706.03794 [hep-ex].

[8] ATLAS Collaboration, *Search for dark matter at* $\sqrt{s} = 13$ *TeV in final states containing an energetic photon and large missing transverse momentum with the ATLAS detector*, Eur. Phys. J. C **77** (2017) 393, arXiv: 1704.03848 [hep-ex].

[9] ATLAS Collaboration, *Search for Dark Matter Produced in Association with a Higgs Boson Decaying to* $b\bar{b}$ *using 36* $fb^{-1}$ *of pp collisions at* $\sqrt{s} = 13$ *TeV with the ATLAS Detector*, Phys. Rev. Lett. **119** (2017) 181804, arXiv: 1707.01302 [hep-ex].

[10] ATLAS Collaboration, *Search for dark matter in association with a Higgs boson decaying to two photons at* $\sqrt{s} = 13$ *TeV with the ATLAS detector*, Phys. Rev. D **96** (2017) 112004, arXiv: 1706.03948 [hep-ex].

[11] ATLAS Collaboration, *Search for new phenomena in final states with an energetic jet and large missing transverse momentum in pp collisions at* $\sqrt{s} = 13$ *TeV using the ATLAS detector*, Phys. Rev. D **94** (2016) 032005, arXiv: 1604.07773 [hep-ex].

[12] CMS Collaboration, *Search for associated production of dark matter with a Higgs boson decaying to* $b\bar{b}$ *or* $\gamma\gamma$ *at* $\sqrt{s} = 13$ *TeV*, JHEP **10** (2017) 180, arXiv: 1703.05236 [hep-ex].

[13] ATLAS Collaboration, *Search for dark matter produced in association with bottom or top quarks in* $\sqrt{s} = 13$ *TeV pp collisions with the ATLAS detector*, Eur. Phys. J. C **78** (2018) 18, arXiv: 1710.11412 [hep-ex].

[14] M. R. Buckley, D. Feld and D. Goncalves, *Scalar Simplified Models for Dark Matter*, Phys. Rev. D **91** (2015) 015017, arXiv: 1410.6497 [hep-ph].

[15] D. Abercrombie et al., *Dark Matter Benchmark Models for Early LHC Run-2 Searches: Report of the ATLAS/CMS Dark Matter Forum*, (2015), ed. by A. Boveia, C. Doglioni, S. Lowette, S. Malik and S. Mrenna, arXiv: 1507.00966 [hep-ex].

[16] U. Haisch and E. Re, *Simplified dark matter top-quark interactions at the LHC*, JHEP **06** (2015) 078, arXiv: 1503.00691 [hep-ph].

[17] M. Bauer, U. Haisch and F. Kahlhoefer,
*Simplified dark matter models with two Higgs doublets: I. Pseudoscalar mediators*,
JHEP **05** (2017) 138, arXiv: 1701.07427 [hep-ph].

[18] T. Abe et al., *LHC Dark Matter Working Group: Next-generation spin-0 dark matter models*, (2018), arXiv: 1810.09420 [hep-ex].

[19] D. Pinna, A. Zucchetta, M. R. Buckley and F. Canelli, *Single top quarks and dark matter*, Phys. Rev. D **96** (2017) 035031, arXiv: 1701.05195 [hep-ph].

[20] ATLAS Collaboration, *The ATLAS Experiment at the CERN Large Hadron Collider*, JINST **3** (2008) S08003.

[21] ATLAS Collaboration, *Technical Design Report for the ATLAS Inner Tracker Strip Detector*, CERN-LHCC-2017-005, 2017, URL: http://cds.cern.ch/record/2257755.

[22] ATLAS Collaboration,
*Technical Design Report for the Phase-II Upgrade of the ATLAS Muon Spectrometer*,
CERN-LHCC-2017-017, 2017, URL: http://cds.cern.ch/record/2285580.

[23] ATLAS Collaboration,
*Technical Design Report for the Phase-II Upgrade of the ATLAS LAr Calorimeter*,
CERN-LHCC-2017-018, 2017, URL: http://cds.cern.ch/record/2285582.

[24] ATLAS Collaboration,
*Technical Design Report for the Phase-II Upgrade of the ATLAS Tile Calorimeter*,
CERN-LHCC-2017-019, 2017, URL: http://cds.cern.ch/record/2285583.

[25] ATLAS Collaboration,
*Technical Design Report for the Phase-II Upgrade of the ATLAS TDAQ System*,
CERN-LHCC-2017-020, 2017, URL: http://cds.cern.ch/record/2285584.

[26] ATLAS Collaboration, *Technical Design Report for the ATLAS Inner Tracker Pixel Detector*, CERN-LHCC-2017-021, 2017, URL: http://cds.cern.ch/record/2285585.

[27] ATLAS Collaboration,
*Technical Proposal: A High-Granularity Timing Detector for the ATLAS Phase-II Upgrade*,
CERN-LHCC-2018-023, 2018, URL: http://cds.cern.ch/record/2623663.

[28] S. Agostinelli et al., *GEANT4: A Simulation toolkit*, Nucl. Instrum. Meth. A **506** (2003) 250.

[29] ATLAS Collaboration, *The ATLAS Simulation Infrastructure*, Eur. Phys. J. C **70** (2010) 823, arXiv: 1005.4568 [physics.ins-det].

[30] ATLAS Collaboration, *Expected performance of the ATLAS detector at the HL-LHC*, 2018 in progress, URL: http://cds.cern.ch/record/.

[31] ATLAS Collaboration, *ATLAS Pythia8 tunes to 7 TeV data*, ATL-PHYS-PUB-2014-021, 2014, URL: http://cds.cern.ch/record/1966419.

[32] S. Frixione, P. Nason and G. Ridolfi,
*A Positive-weight next-to-leading-order Monte Carlo for heavy flavour hadroproduction*,
JHEP **09** (2007) 126, arXiv: 0707.3088 [hep-ph].

[33] P. Nason, *A New method for combining NLO QCD with shower Monte Carlo algorithms*, JHEP **11** (2004) 040, arXiv: hep-ph/0409146 [hep-ph].

[34] S. Frixione, P. Nason and C. Oleari,
*Matching NLO QCD computations with Parton Shower simulations: the POWHEG method*,
JHEP **11** (2007) 070, arXiv: 0709.2092 [hep-ph].

[35] T. Sjöstrand, S. Mrenna and P. Z. Skands, *A Brief Introduction to PYTHIA 8.1*,
Comput. Phys. Commun. **178** (2008) 852, arXiv: 0710.3820 [hep-ph].

[36] H.-L. Lai et al., *New parton distributions for collider physics*, Phys. Rev. D **82** (2010) 074024,
arXiv: 1007.2241 [hep-ph].

[37] N. Kidonakis, *Next-to-next-to-leading-order collinear and soft gluon corrections for t-channel single top quark production*, Phys. Rev. D **83** (2011) 091503, arXiv: 1103.2792 [hep-ph].

[38] N. Kidonakis,
*Two-loop soft anomalous dimensions for single top quark associated production with a W- or H-*,
Phys. Rev. D **82** (2010) 054018, arXiv: 1005.4451 [hep-ph].

[39] N. Kidonakis, *NNLL resummation for s-channel single top quark production*,
Phys. Rev. D **81** (2010) 054028, arXiv: 1001.5034 [hep-ph].

[40] J. Alwall et al., *The automated computation of tree-level and next-to-leading order differential cross sections, and their matching to parton shower simulations*, JHEP **07** (2014) 079,
arXiv: 1405.0301 [hep-ph].

[41] T. Gleisberg et al., *Event generation with SHERPA 1.1*, JHEP **02** (2009) 007,
arXiv: 0811.4622 [hep-ph].

[42] G. Corcella et al., *HERWIG 6: An Event generator for hadron emission reactions with interfering gluons (including supersymmetric processes)*, JHEP **01** (2001) 010, arXiv: hep-ph/0011363.

[43] LHC Higgs Cross Section Working Group,
*Handbook of LHC Higgs Cross Sections: 2. Differential Distributions*,
CERN-2012-002 (CERN, Geneva, 2012), arXiv: 1201.3084 [hep-ph].

[44] J. Pumplin et al.,
*New generation of parton distributions with uncertainties from global QCD analysis*,
JHEP **07** (2002) 012, arXiv: hep-ph/0201195.

[45] T. Gleisberg, S. Hoeche, F. Krauss, M. Schonherr, S. Schumann et al.,
*Event generation with SHERPA 1.1*, JHEP **02** (2009) 007, arXiv: 0811.4622 [hep-ph].

[46] S. Catani, L. Cieri, G. Ferrera, D. de Florian and M. Grazzini,
*Vector boson production at hadron colliders: a fully exclusive QCD calculation at NNLO*,
Phys. Rev. Lett. **103** (2009) 082001, arXiv: 0903.2120 [hep-ph].

[47] M. Cacciari, G. P. Salam and G. Soyez, *The anti-$k_t$ jet clustering algorithm*, JHEP **04** (2008) 063,
arXiv: 0802.1189 [hep-ph].

[48] ATLAS Collaboration, *ATLAS Phase-II Upgrade Scoping Document*,
CERN-LHCC-2015-020. LHCC-G-166, 2015, URL: http://cds.cern.ch/record/2055248.

[49] ATLAS Collaboration,
*Measurements of b-jet tagging efficiency with the ATLAS detector using $t\bar{t}$ events at $\sqrt{s} = 13$ TeV*,
JHEP **08** (2018) 089, arXiv: 1805.01845 [hep-ex].

[50] ATLAS Collaboration, *Performance of b-Jet Identification in the ATLAS Experiment*,
JINST **11** (2016) P04008, arXiv: 1512.01094 [hep-ex].

[51] ATLAS Collaboration, *Optimisation of the ATLAS b-tagging performance for the 2016 LHC Run*, ATL-PHYS-PUB-2016-012, URL: https://cds.cern.ch/record/2160731.

[52] ATLAS Collaboration, *Electron reconstruction and identification efficiency measurements with the ATLAS detector using the 2011 LHC proton–proton collision data*, Eur. Phys. J. C **74** (2014) 2941, arXiv: 1404.2240 [hep-ex].

[53] ATLAS Collaboration, *Electron identification measurements in ATLAS using* $\sqrt{s} = 13$ *TeV data with* 50 *ns bunch spacing*, ATL-PHYS-PUB-2015-041, 2015, URL: https://cds.cern.ch/record/2048202.

[54] ATLAS Collaboration, *Measurement of the muon reconstruction performance of the ATLAS detector using 2011 and 2012 LHC proton–proton collision data*, Eur. Phys. J. C **74** (2014) 3130, arXiv: 1407.3935 [hep-ex].

[55] ATLAS Collaboration, *Muon reconstruction performance of the ATLAS detector in proton–proton collision data at* $\sqrt{s} = 13$ *TeV*, Eur. Phys. J. C **76** (2016) 292, arXiv: 1603.05598 [hep-ex].

[56] ATLAS Collaboration, *Search for direct top-squark pair production in final states with two leptons in pp collisions at* $\sqrt{s} = 8$ *TeV with the ATLAS detector*, JHEP **06** (2014) 124, arXiv: 1403.4853 [hep-ex].

[57] C. G. Lester and D. J. Summers, *Measuring masses of semiinvisibly decaying particles pair produced at hadron colliders*, Phys. Lett. B **463** (1999) 99, arXiv: hep-ph/9906349.

[58] A. Barr, C. Lester and P. Stephens, *m(T2) : The Truth behind the glamour*, J. Phys. G **29** (2003) 2343, arXiv: hep-ph/0304226.

[59] W. S. Cho, K. Choi, Y. G. Kim and C. B. Park, *Measuring superparticle masses at hadron collider using the transverse mass kink*, JHEP **02** (2008) 035, arXiv: 0711.4526 [hep-ph].

[60] M. Burns, K. Kong, K. T. Matchev and M. Park, *Using Subsystem MT2 for Complete Mass Determinations in Decay Chains with Missing Energy at Hadron Colliders*, JHEP **03** (2009) 143, arXiv: 0810.5576 [hep-ph].

[61] M. Baak et al., *HistFitter software framework for statistical data analysis*, Eur. Phys. J. C **75** (2015) 153, arXiv: 1410.1280 [hep-ex].

[62] G. Cowan, K. Cranmer, E. Gross and O. Vitells, *Asymptotic formulae for likelihood-based tests of new physics*, Eur. Phys. J. C **71** (2011) 1554, [Erratum: Eur. Phys. J. C **73** (2013) 2501], arXiv: 1007.1727 [physics.data-an].

[63] A. L. Read, *Presentation of search results: The CL(s) technique*, J. Phys. G **28** (2002) 2693.

[64] A. Boveia et al., *Recommendations on presenting LHC searches for missing transverse energy signals using simplified s-channel models of dark matter*, (2016), arXiv: 1603.04156 [hep-ex].

[65] LUX Collaboration, *Results on the Spin-Dependent Scattering of Weakly Interacting Massive Particles on Nucleons from the Run 3 Data of the LUX Experiment*, Phys. Rev. Lett. **116** (2016) 161302, arXiv: 1602.03489 [hep-ex].

[66] LUX Collaboration, *Results from a Search for Dark Matter in the Complete LUX Exposure*, Phys. Rev. Lett. **118** (2017) 021303, arXiv: 1608.07648 [astro-ph.CO].

[67] CRESST Collaboration, *First results on low-mass dark matter from the CRESST-III experiment*, (2017), arXiv: 1711.07692 [astro-ph.CO].

[68] XENON Collaboration, *Dark Matter Search Results from a One Ton-Year Exposure of XENON1T*, Phys. Rev. Lett. **121** (2018) 111302, arXiv: 1805.12562 [astro-ph.CO].

[69] PandaX-II Collaboration,
*Dark Matter Results from First 98.7 Days of Data from the PandaX-II experiment*,
Phys. Rev. Lett. **117** (2016) 121303, arXiv: 1607.07400 [hep-ex].

[70] DarkSide Collaboration, *Low-Mass Dark Matter Search with the DarkSide-50 Experiment*, Phys. Rev. Lett. **121** (2018) 081307, arXiv: 1802.06994 [astro-ph.HE].